# Electronic Spectroscopy of the Halogenated Criegee Intermediate, ClCHOO: Experiment and Theory

Elizabeth Karlsson[a], Rawan Rabayah[a], Tianlin Liu[a,*], Emmanuel Moya Cruz[a], Marisa C. Kozlowski[a], Tolga N. V. Karsili[b], Marsha I. Lester[a,†]
[a] Department of Chemistry, University of Pennsylvania, Philadelphia, PA 19104-6323 USA
[b] Department of Chemistry, University of Louisiana, Lafayette, LA, 70504 USA

## Abstract

A chlorine-substituted Criegee intermediate, ClCHOO, is photolytically generated using a diiodo precursor, detected by VUV photoionization at 118 nm, and spectroscopically characterized via ultraviolet-visible (UV-vis)-induced depletion of m/z = 80 under jet cooled conditions. UV-vis excitation resonant with a $\pi^* \leftarrow \pi$ transition yields a significant ground state depletion, indicating a strong electronic transition and rapid photodissociation. The broad absorption spectrum peaks at 350 nm and is attributed to contributions from both *syn* (~70%) and *anti* (~30%) conformers of ClCHOO based on spectral simulations using a nuclear ensemble method. Electronic structure theory shows significant differences in the vertical excitation energies of the two conformers (330 and 371 nm, respectively) as well as their relative stabilities in the ground and excited electronic states associated with the $\pi^* \leftarrow \pi$ transition. Natural bond orbital analysis reveals significant and non-intuitive non-bonding contributions to the relative stabilities of the *syn* and *anti* conformers.

[*] Current address: Department of Chemistry and Biochemistry, University of California San Diego, La Jolla, CA 92093
[†] Corresponding author email: milester@sas.upenn.edu

## Introduction

Alkenes are important unsaturated species that are emitted into the atmosphere from both anthropogenic and biogenic sources. Atmospheric ozonolysis of alkenes generates zwitterionic carbonyl oxide intermediates ($R_1R_2C{=}O^{+}{-}O^{-}$) known as Criegee intermediates. As alkene structures vary widely, Criegee intermediates with different structural motifs and conformations are formed. Isoprene-derived Criegee intermediates, formaldehyde oxide ($CH_2OO$), methyl vinyl ketone oxide ($(CH_2{=}CH)(CH_3)COO$), and methacrolein oxide ($CH_2{=}C(CH_3))CHOO$),[1-3] have been studied extensively as isoprene emissions are estimated to be up to 600 TgC $year^{-1}$.[4] Ozonolysis of asymmetrically substituted alkenes such as propene and butene yield alkyl substituted carbonyl oxides ($CH_3CHOO$ and $CH_3CH_2CHOO$, respectively).[5, 6] As Criegee intermediates generated from ozonolysis are formed with high internal energy, prompt ground state unimolecular decay is expected to account for up to 50% loss of initially generated Criegee intermediates.[7] Upon collisional stabilization, carbonyl oxide sinks include thermal unimolecular decay, bimolecular reactions, and photodissociation. The substituents and conformation of Criegee intermediates have been shown to yield drastically different unimolecular decay and bimolecular processes with rates that can differ by orders of magnitude.[8-10]

Criegee intermediates resulting from ozonolysis of heteroatom-substituted unsaturated hydrocarbons are far less characterized. This study investigates the simplest singly chlorinated carbonyl oxide, ClCHOO. ClCHOO is a model system intended to probe the σ and π perturbing effects of a Cl substituent on the carbonyl oxide group. Further, haloalkenes emissions are primarily anthropogenic as they are used for various industrial purposes; in particular, hydrofluoroolefins (HFOs) and hydrochlorofluoroolefins (HCFOs) are currently being implemented as 4$^{th}$ generation refrigerants. The primary atmospheric sink for HCFOs is oxidation by hydroxyl radicals, and atmospheric studies have begun identifying decay products associated with this process.[11] Ozonolysis of HFOs and HCFOs contribute to their atmospheric loss in environments containing high ozone concentration – such as urban areas where refrigerant emissions occur.[7, 12] Ozonolysis of the refrigerant HFO-1234ze(E) produces fluoroform ($CHF_3$), an

extremely long-lived species with a high global warming potential (GWP).[13] One such Criegee intermediate that is expected to be generated from ozonolysis of haloalkenes ($HClC=C(H)CF_3$, $HClC=C(F)CF_3$) is the singly chlorinated Criegee intermediate, ClCHOO. ClCHOO has been studied previously both computationally and experimentally. Kumar and Francisco computationally probed ClCHOO bimolecular reactions with $CO_2$ and H–X (X = H, $CH_3$, $CH_2F$, $CHF_2$, $CF_3$, and $SiH_3$) and found a significant difference in reactivity between *syn* and *anti* conformers of ClCHOO.[14, 15] Cabezas et al. characterized the electronic ground state of ClCHOO using Fourier-transform microwave (FTMW) spectroscopy.[16]

Electronic spectroscopy of Criegee intermediates has been probed for multiple carbonyl oxide systems, as it provides a sensitive means of detection and characterizes their photochemical processes in the atmosphere.[17] Further, ultraviolet-visible (UV-vis) absorption gives insight to ground and excited state electronic structure. For instance, extended conjugation, orbital overlap, and ground state relative stability can give rise to large shifts in electronic spectra across Criegee intermediates and their conformers.[18] Transient UV-vis absorption is also widely utilized to monitor Criegee intermediate populations in ground state unimolecular and bimolecular reaction kinetic studies.[19] Kapnas et al. reported a transient absorption spectrum of ClCHOO that captured a portion of the electronic spectrum from 345 to 440 nm under thermal conditions.[20] In the present study, the full absorption spectrum of ClCHOO on the strong $\pi^* \leftarrow \pi$ transition is obtained under jet-cooled conditions. The ground and optically bright electronic excited states of ClCHOO are investigated theoretically and are found to have large conformational dependencies. Single and multi- reference theoretical methods are used to probe the ground state and electronically excited state energetics, respectively.

## Experimental Methods

ClCHOO is produced from a chlorodiiodomethane ($ClCHI_2$) precursor. A detailed procedure of the synthesis of $ClCHI_2$ has been reported previously.[21] An alternative purification method is utilized as detailed in the Supporting Information (SI). ClCHOO is generated in a quartz

capillary reactor tube and jet-cooled in a pulsed supersonic expansion. The experimental procedures used to produce various Criegee intermediates in this laboratory have been described previously.[1, 5, 22] Briefly, the precursor is heated (58 °C), seeded in a 20% $O_2$/Ar carrier gas (15 psig), and pulsed through a solenoid valve into a quartz capillary tube reactor (25 mm length; 1 mm ID). The precursor is photolyzed by the 248 nm output (ca. 50 mJ/pulse) from a KrF excimer laser (Coherent, Compex 102), which is cylindrically focused along the capillary. The resultant monoiodo radical subsequently reacts with $O_2$ to produce ClCHOO. ClCHOO is collisionally stabilized within the capillary and cooled in the ensuing supersonic expansion to a rotational temperature of ~10 K.[23, 24]

For photoionization measurements, the gas mixture travels ~5 cm downstream where it is crossed by focused VUV radiation (118 nm) that is generated by frequency tripling the third harmonic output of a Nd:YAG laser in a phase matched Xe:Ar gas mixture. The $ClCHOO^+$ mass channel (m/z = 80) is detected using a time-of-flight (TOF) mass spectrometer.

UV-vis radiation is generated using a broadly tunable β-barium borate-optical parametric oscillator (BBO-OPO) source (EKSPLA 342NT; 5 $cm^{-1}$ linewidth). The sum frequency generation (SFG) of the signal output and the Nd:YAG fundamental is utilized between 295 and 409 nm. UV-vis radiation is introduced as an unfocused beam that spatially overlaps the counter-propagating VUV radiation. The OPO excitation (5 Hz) is introduced ~40 ns before VUV photoionization (10 Hz).

**Theoretical Methods**

The ground state minimum energy geometries and anharmonic frequencies of *syn*-ClCHOO, *anti*-ClCHOO, and $CH_2OO$ were obtained using the B2PLYP-D3 coupled with Dunning's augmented correlation consistent basis set of triple-ζ quality: aug-cc-pVTZ using Gaussian 16. [25]

Natural bond orbital (NBO) analysis was carried out on these optimized geometries.[26] In addition, the transition state barrier associated with isomerization between between *syn*-ClCHOO and *anti*-ClCHOO as well as the vertical (VIE) and adiabatic (AIE) ionization energies were evaluated at this same level of theory. The VIE is the energy difference between the cation and the neutral species in the ground state minimum energy geometry. The AIE is the minimum energy required to remove an electron from the neutral species combined with the difference in zero-point energy between the cation and the neutral species. AIEs of other possible isomers of ClCHOO were calculated at B2PLYP-D3/aug-cc-pVTZ level. Single-point energies on the optimized *syn*-ClCHOO and *anti*-ClCHOO structures were computed at the CCSD(T)-F12/cc-pVTZ-F12 level using the Molpro computational package.[27-30] Further multireference calculations were done using Molpro. Vertical excitation energies (VEE) of the six lowest singlet excited states were calculated using the single state Complete Active Space Second Order Perturbation theory (CASPT2) coupled with the aug-cc-pVTZ basis set.[31] The CASPT2/aug-cc-pVTZ calculations are based on a seven-singlet state averaged Complete Active Space-Self Consistent Field (SA7-CASSCF) reference wavefunction using the same basis set. Calculations were completed using an active space of 10 electrons in 8 orbitals (10/8) for ClCHOO and $CH_2OO$. Additional CASPT2 calculations were completed using a larger active space consisting of 12 electrons in 9 orbitals (12/9) for ClCHOO to account for an additional nonbonding orbital centered on the Cl atom.[32] The active space orbitals are presented in Supporting Information (Figure S3). This active space ensures a balanced description of relevant excited states of Criegee intermediates within the experimentally probed energy range at a reasonable computational cost.[22] An imaginary shift of 0.5 $E_H$ is applied to the CASPT2 calculations to aid

convergence and mitigate the involvement of intruder states. Oscillator strengths ($f_{ij}$) for the lowest spin allowed transitions are calculated using the CASSCF transition dipole moments ($\mu_{ij}$)

$$f_{ij} = \frac{2}{3} E_{ij} \sum_{a=x,y,z} \left|\mu_{ij}\right|_{\alpha}^{2}$$

associated with the electronic transition from state *i* (electronic ground state) to state *j* (7 lowest energy electronic excited states) with CASPT2 energies ($E_{ij}$). Additionally, unrelaxed potential energy profiles of ClCHOO along the O-O stretch coordinate ($R_{O\text{-}O}$) were calculated at the CASPT2/aug-cc-pVTZ level of theory with the (12/9) active space.

Absorption spectra for *syn*- and *anti*-ClCHOO conformers were simulated using the nuclear ensemble method.[33] 300 Wigner geometries were generated around the optimized ground state geometry of each conformer using Newton-X.[34, 35] These were based on the associated ground state normal mode harmonic frequencies. The oscillator strengths ($f_{ij}$) and VEE ($E_{ij}$) for the six lowest lying spin allowed transitions were computed using CASSCF(12,9)/CASPT2(12,9)/aug-cc-pVTZ level of theory with the (10/8) and (12/9) active space. An energy dependent absorption cross-section $P(E)$ is determined by summing over the resulting VEEs and oscillator strengths of all 300 Wigner geometries and the final states of interest (M), which includes transitions from initial state *i* (ground state) to final state *j* (i.e., S1, S2, S3, ..., S7)

$$P(E) = \frac{\pi e^2}{2 m_e c \varepsilon_0} \sum_{j=1}^{M} \left[ \frac{1}{N_{tot}} \sum_{N=1}^{N_{tot}} f_{ij}^{N} g\left(E - \Delta E_{ij}^{N}, \delta\right) \right]$$

and where $m_e$ and $e$ are the mass and charge of an electron, $c$ is the speed of light, $\varepsilon_0$ is the vacuum permittivity. A Lorentzian line shape $g(E\text{-}\Delta E)$ is given by:

$$g\left(E - \Delta E_{ij}^{N}, \delta\right) = \frac{\hbar \delta}{2\pi} \left( \left(E - \Delta E_{ij}^{N}\right)^2 + \left(\frac{\delta}{2}\right)^2 \right)^{-1}$$

Here, δ is an artificial broadening factor (0.1 eV) and $\hbar$ is the reduced Planck's constant.

**Results and Discussion**

The minimum energy geometries of *syn*-ClCHOO, *anti*-ClCHOO and $CH_2OO$ are presented in Figure 1. The conformers are distinguishable by whether the terminal oxygen is oriented towards or away from the Cl substituent. The *syn* conformer is 2.6 kcal $mol^{-1}$ more stable than the *anti* conformer. The barrier to isomerization is 24.0 kcal $mol^{-1}$, indicating that *syn*- and *anti*-ClCHOO can be treated as separate species under jet cooled conditions. Calculated ionization thresholds (AIE) of 9.6 eV and 9.4 eV for the *syn* and *anti* conformers, respectively, are below 10.5 eV, and thus the photoionization detection scheme utilized is expected to detect the m/z = 80 mass channel. More stable isomers (Table S1) such as chlorodioxirane (calculated AIE = 10.8 eV) or chloroformic acid isomers (calculated AIE > 11.4 eV), if formed, are not expected to be ionized with 10.5 eV radiation.

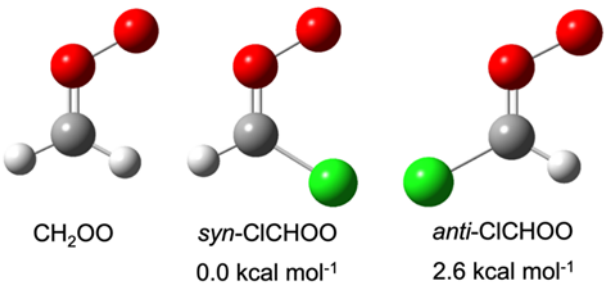


**Figure 1.** Ground state geometries optimized at the B2PLYP-D3/aug-cc-pVTZ level of theory for $CH_2OO$, *syn*-ClCHOO and *anti*-ClCHOO. Relative energies of ClCHOO conformers are determined from zero-point-corrected single-point energies calculated at the CCSD(T)-F12/cc-pVTZ-F12 level of theory.

CASPT2 calculations for both *syn*- and *anti*-ClCHOO (Table S2) predict the lowest electronically excited state ($S_1$) to have $n\pi^*$ character with negligible oscillator strength and is therefore expected to be optically dark under the present experimental conditions. In contrast, excitation to the $S_2$ state involves a strongly absorbing $\pi^* \leftarrow \pi$ transition as found for prototypical Criegee intermediates, such as $CH_2OO$, previously studied.[1, 17] The vertical excitation energies

(VEEs) and corresponding oscillator strengths for $CH_2OO$ and *syn*- and *anti*- ClCHOO were calculated at the CASPT2(10/8) and CASPT2(12/9) levels of theory, respectively, and are presented in Table 1. The larger active space in the latter arises from the addition of a Cl centered $3p_x$ orbital, which was motivated by the configuration interaction (CI) coefficients that expectedly showed contribution from a Cl centered valence orbital. Calculated VEEs with and without this orbital for both *syn*- and *anti*-ClCHOO are given in Table S3.

The experimental UV-vis depletion scheme is illustrated on the (unrelaxed) potential energy profiles computed for *syn*-ClCHOO in Figure 2 (left panel). Guided by the VEEs in Table 1, irradiation of ClCHOO in the UV-vis range is expected to electronically excite ClCHOO to the

**Table 1.** Vertical excitation energies and oscillator strengths for $CH_2OO$, *syn*-ClCHOO and *anti*-ClCHOO on the $S_2 \leftarrow S_0$ electronic transition at the CASPT2(12/9)/AVTZ and CASPT2(10/8)/AVTZ level of theory for $CH_2OO$ and ClCHOO, respectively.

| | Vertical Excitation Energy | Oscillator Strength |
|---|---|---|
| $CH_2OO$ | 3.78 eV (328 nm) | 0.102 |
| *syn*-ClCHOO | 3.76 eV (330 nm) | 0.107 |
| *anti*-ClCHOO | 3.33 eV (371 nm) | 0.106 |

optically bright $S_2$ state. As illustrated previously,[36, 37] the diabatic $1^1\pi\pi^*$ state is strongly coupled to a near-lying potential energy surface that is dissociative along the O–O coordinate, which correlates to the lowest spin-allowed ClCHO $X^1A'$ + O $^1D$ products. $CH_2OO$ and other prototypical Criegee intermediates have been shown to undergo similar prompt O–O fission to singlet carbonyl + O $^1D$ products following UV-vis excitation.[37-39]

UV-vis spectroscopy of ClCHOO is achieved using a UV-vis depletion method described previously.[6, 22, 40] Inherent to this method is the assumption of prompt (ps) photodissociation, as demonstrated experimentally by velocity map imaging and theoretically by trajectory studies for

$CH_2OO$ (as well as several alkyl-substituted Criegee intermediates).[38, 41, 42] Following UV-vis excitation, a 118 nm laser pulse with a time delay of ca. 40 ns ionizes any remaining ground state ClCHOO molecules. Resonant electronic excitation of *syn*- and *anti*-ClCHOO is observed as a UV-vis induced depletion of the ground state population of the corresponding conformer. The resultant ground state depletion is detected as a reduced VUV photoionization signal at m/z = 80. Figure 2 (right panel) shows a representative ground state depletion in which resonant UV-vis excitation induces a significant decrease in the VUV photoionization signal. Chlorine has two isotopes with natural abundances of ~75% and ~25% population for $^{35}Cl$ and $^{37}Cl$, respectively. As a result, photoionization is observed on two mass channels with analogous percentage UV-vis-induced depletions. The larger $^{35}$ClCHOO photoionization signal was monitored for the depletion measurements.

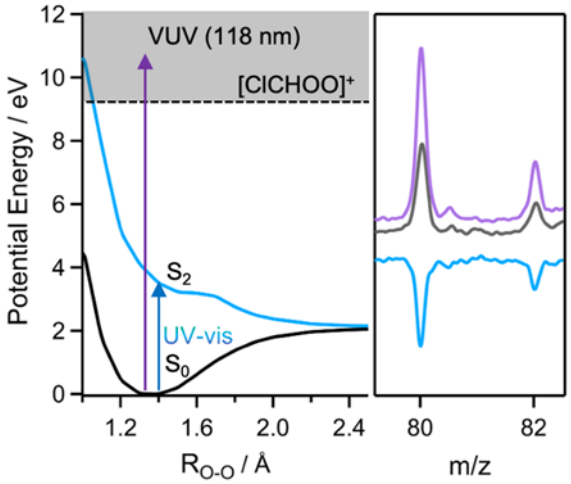


**Figure 2**. (Left panel) Potential energy curves (unrelaxed) along the O–O bond dissociation coordinates for the ground $S_0$ and optically bright $S_2$ states of *syn*-ClCHOO. UV-vis excitation to the repulsive $S_2$ excited state results in a reduction of the ground state population and associated depletion in the VUV photoionization signal. (Right panel) Mass spectrum arising from photoionization of ClCHOO isotopologues $^{35}$ClCHOO (m/z = 80) and $^{37}$ClCHOO (m/z = 82). The purple trace (top) shows the VUV only ionization signal, while the overlaid gray (middle) trace illustrates a significant reduction in the VUV photoionization signal upon UV excitation at 350 nm. The blue trace (bottom) shows the depleted VUV signal upon UV excitation.

The VUV laser operates at 10 Hz while the BBO-OPO operates at 5 Hz to obtain the UV-vis induced fractional depletion [(UV-vis off – UV-vis on) / (UV-vis off)] on the parent mass channel (m/z = 80). The percentage depletion, expressed as $[(N_0 - N) / (N_0)] \times 100\%$, with ground state abundance (**$N_0$**) before and (**N**) after UV-vis irradiation, increases linearly with UV-vis power to a maximum depletion of 60% at 340 nm (Figure S4). A significant ground state depletion is indicative of a strong electronic transition. This reflects the significant oscillator strength computed for both *syn*- and *anti*-ClCHOO and is similar to previously studied Criegee intermediates.[40, 43] The corresponding absorbance, $-\ln (N/N_0)$, scales linearly with UV-vis power up to 2.6 mJ/pulse in the SFG range, indicating a one-photon process (Figure S4).

The resultant electronic spectrum of ClCHOO recorded in the UV-vis range from 295 to 409 nm is shown in Figure 3. The OPO power is maintained between 2.0–2.5 mJ/pulse throughout the region, which is within the linear power regime. The averaged data points from repeated measurements (1500 OPO pulses) are normalized by power. The gray shading accounts for $\pm 1\sigma$ uncertainty in measurements. The experimental spectrum is broad and symmetrical with a peak centered at 350 nm and a FWHM of 70 nm. The spectrum agrees well with the partial transient absorption spectrum reported by Kapnas et al. from 345 to 440 nm (green).[20] Further, Kapnas et al. reported an estimated absorption cross section over their spectral range with an absorption cross section of $\sim 7.3 \times 10^{-18}$ cm$^2$ at 350 nm for ClCHOO. By comparison, the $CH_2OO$ spectrum recorded under similar conditions by Beames et al. peaks at 335 nm with a FWHM of ca. 40 nm;[1] $CH_2OO$ has an absorption cross section of $1.23 \times 10^{-17}$ cm$^2$ at 340 nm as reported by Ting et al.[44] Predicted VEEs for both *syn*- and *anti*-ClCHOO fall within the spectral range of the broad absorption spectrum, indicating that both conformers may be contributing to the absorbance.

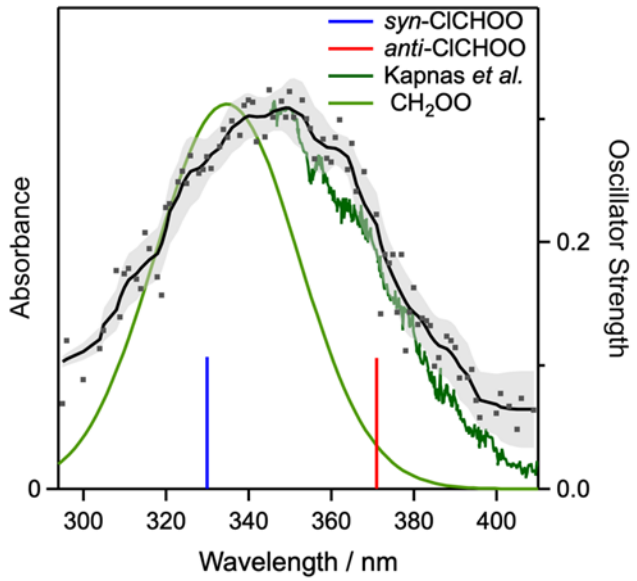


**Figure 3**. Experimental UV-vis spectrum of ClCHOO from 295–409 nm derived from depletion of the VUV photoionization signal on m/z = 80. The solid line through the data points is a smoothed fit (4 point) with ± 1σ uncertainty indicated by the gray shaded region. The previously reported absorption spectrum of ClCHOO (dark green) is reproduced with permission from Ref. 20. Copyright 2017 Royal Society of Chemistry. The previously reported UV spectrum of $CH_2OO$ (light green) recorded under similar experimental conditions on m/z = 46 by Beames et al. is reproduced from Ref. 1. Copyright 2012 American Chemical Society. The peak intensities of the spectra are set equal for comparison. Also shown are the computed CASPT2(12,9)/aug-cc-pVTZ VEEs and associated oscillator strengths on the $\pi^* \leftarrow \pi$ transition for *syn* (blue) and *anti* (red) conformers of ClCHOO (bars).

For comparison, the electronic spectra for *syn*- and *anti*-ClCHOO were simulated over a 250–450 nm range using the nuclear ensemble method and the CASPT2/CASSCF(12/9) results are shown in Figure 4.[33] The simulation indicates that absorption over the 250–450 nm region is dominated by partially overlapping $\pi^* \leftarrow \pi$ transitions of the *syn* and *anti* conformers. The spectral breadth of each conformer reflects the Frank-Condon profile associated with the 300 initial geometries (Figure S5). The absorption maxima of the simulations for *syn*- and *anti*-ClCHOO are 342 nm and 365 nm, respectively. The calculated peak absorption cross sections for *syn*- and *anti*-ClCHOO are $1.21\times10^{-17}$ cm$^2$ and $1.41\times10^{-17}$ cm$^2$, respectively. As described above, including the $3p_x$ orbital in the active space of ClCHOO is essential as this orbital conjugates and extends resonance with the COO centered π-system. This is evident in the

spectral simulations of the *syn* conformer, where utilizing the (12/9) active space with the added nonbonding orbital on the Cl atom yields improved agreement with experiment, particularly on the short wavelength side, than the (10/8) active space (see Figure S6).

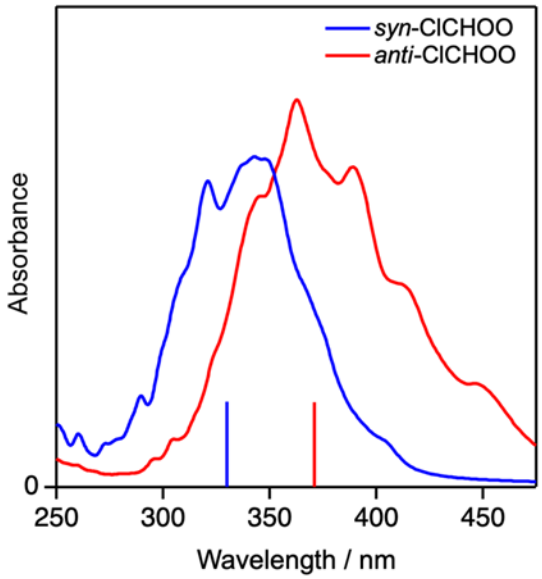


**Figure 4.** Calculated electronic absorption spectra for *syn* (blue) and *anti* (red) conformers of ClCHOO with corresponding VEEs and oscillator strengths (bars) at the CASPT2(12/9)/AVTZ level of theory.

Cabezas and coworkers reported an estimated 30% population for the higher energy *anti*-conformer in FTMW studies of ClCHOO under jet cooled conditions based on observed spectral intensities.[16] An analogous conformer population ratio is assumed under the present jet-cooled experimental conditions. Figure 5 shows a composite simulated spectrum comprising the summation of 70% *syn*-ClCHOO and 30% *anti*-ClCHOO components. The composite spectrum has a larger breadth than the simulation of the *syn* conformer alone, and has an absorption maximum at 350 nm. The experimental and the composite simulated spectra are compared in the region from 295 to 409 nm as shown in Figure 5. The experimental and theoretical composite spectra are in agreement regarding the absorption maxima. Further, the breadth and fall off to longer and shorter wavelengths agree well. This is most likely due to jet-cooled conditions

producing a population distribution that closely resembles a Wigner distribution as the latter models the ground vibrational level of the $S_0$ electronic state. Therefore, the experimental spectrum is attributed to both *syn* and *anti* conformers of ClCHOO with an assumed ~70:30 population ratio.

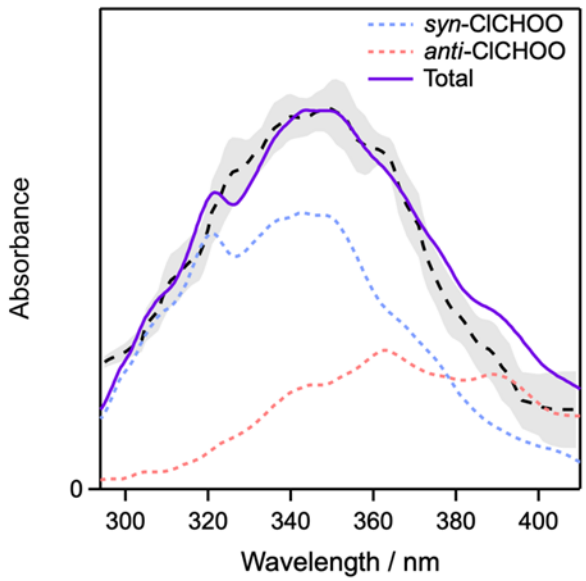


**Figure 5.** Experimental UV-vis spectrum of ClCHOO and the composite calculated spectrum (purple) composed of 70% and 30% population for *syn*- and *anti*-ClCHOO, respectively.

NBO analysis was carried out on *syn*-ClCHOO, *anti*-ClCHOO, and $CH_2OO$ to probe the underlying electronic properties contributing to the relative stabilities of each species in its ground electronic state. Table 2 shows relevant donor-acceptor interactions in these systems. Consistent with previous studies of Criegee intermediates, significant stabilization of ClCHOO arises from electron donation into the π backbone of the molecule.[45, 46] Both conformers of ClCHOO are stabilized by a lone pair on the terminal oxygen as well as a lone pair on the chlorine, both of which donate into the antibonding $\pi^*$ C=O orbital (Figure 6). The interaction

energy of oxygen lone pair donation to the antibonding π C=O orbital in the *syn*-ClCHOO conformer is comparable with $CH_2OO$. Both interaction pairs are stronger in the *syn* conformer, and these values agree well with those reported by Cabezas and coworkers.[16]

**Table 2.** Selected NBO stabilization energies (kcal $mol^{-1}$) for ClCHOO conformers and $CH_2OO$.

| Donor | Acceptor | $CH_2OO$ | *syn*-ClCHOO | *anti*-ClCHOO |
|---|---|---|---|---|
| LP[a] O term | π* (C=O) | 49.77 | 47.8 | 39.39 |
| LP Cl | π* (C=O) | - | 38.91 | 34.56 |
| LP O terminal | σ* (C–O) | 7.89 | 8.72 | 6.43 |
| LP O center | σ* (C–Cl) | - | 11.72 | 2.12 |
| σ (O–O) | σ* (C–Cl) | 0.86[b] | 0.72 | 5.83 |
| σ (C–H) | σ* (O–O) | 6.63[c] | 6.28 | <0.5 |

[a] LP refers to lone pair.
[b] Refers to the analogous σ* (C–H) acceptor in the *cis* position of $CH_2OO$.
[c] Refers to the analogous σ* (C–H) donor in the *trans* position of $CH_2OO$.

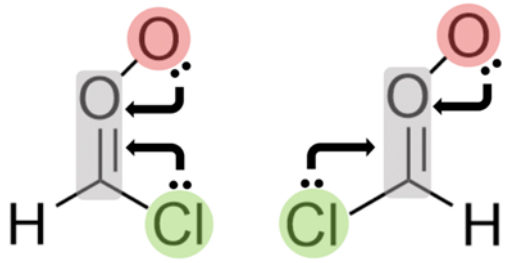


**Figure 6.** Delocalization of electron density from lone pairs of the terminal oxygen (red) and chlorine (green) into the antibonding π* orbital of C=O (gray) stabilize both the *syn*-conformer (left) and the *anti*-conformer (right).

NBO analysis also shows an antiperiplanar nonbonding interaction involving the σ(C–H) and σ*(O–O) orbitals in *syn*-ClCHOO, which is absent in the *anti*-conformer (Table 2). This hyperconjugation-like interaction is also present in $CH_2OO$. In Figure 7, the σ(C–H) and σ*(O–O) orbitals are superimposed for *syn*-ClCHOO, *anti*-ClCHOO, and each of the hydrogens of $CH_2OO$. For $CH_2OO$, significant overlap of the donor and acceptor orbitals occurs when the hydrogen is *trans* to the carbonyl oxide, while overlap is minimal when the hydrogen is in the *cis* position. Hyperconjugation is expected to shorten sigma bonds, and this is consistent with what

has been theoretically predicted and experimentally observed in $CH_2OO$.[47, 48] *Anti*-ClCHOO has a similar carbon-halogen negative hyperconjugative-like force, in which the σ(O-O) bonding orbital donates into the σ(C–Cl) antibonding orbital. However, the σ*(C-Cl) orbital has significantly less spatial overlap with the σ(O–O) bonding orbital compared to a σ(C–H) orbital. Therefore, the stabilization energy for σ(O–O) donation to σ*(C–Cl) (5.83 kcal $mol^{-1}$) is weaker than the energy associated with the nonbonding interaction present in the σ(C–H) bonding orbitals. Cabezas et al. identified that the electronic structure of *syn*-ClCHOO is more similar to $CH_2OO$ than *anti*-ClCHOO, which is also found in the present study. A chlorine in the *trans* position to the C=O bond (instead of a hydrogen) breaks the stabilizing hyperconjugative donation interaction. This antiperiplanar effect is strong in $CH_2OO$ and *syn*-ClCHOO and may play a significant role in the stability of other singly substituted Criegee intermediates. These nonbonding effects may also play a role in the unimolecular decay of ClCHOO and contribute to the strongly conformer-dependent bimolecular reactions rates predicted for *syn*- and *anti*-ClCHOO by Kumar and Francisco.[14, 15]

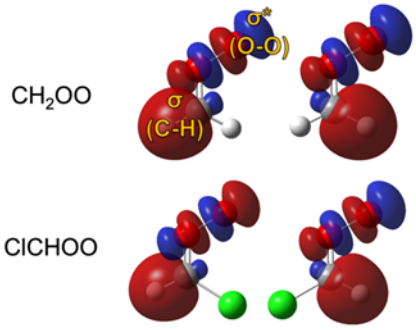


**Figure 7.** Natural bond orbitals corresponding to the σ*(O–O) and σ(C–H) bonds superimposed upon $CH_2OO$ (top), *syn*-ClCHOO (left), and *anti*-ClCHOO (right) structures.

While *syn*-ClCHOO is more stable than *anti*-ClCHOO in the ground state, the calculated $S_2$ energies show the reverse, i.e. that *syn*-ClCHOO is higher in energy than *anti*-ClCHOO. This trend is consistent with $CH_3CHOO$, where destabilization of *syn*-$CH_3CHOO$ in the $S_2$ state was

attributed to extended electron density from the carbonyl oxide onto the methyl hydrogens.[5, 49] The dominant $\pi^* \leftarrow \pi$ orbitals involved in the optically bright $S_2$ state for $CH_2OO$, *syn*-ClCHOO, and *anti*-ClCHOO are shown in Figure 8**.** Extended electron density across chlorine is evident in the $\pi$ and $\pi^*$ orbitals of both conformers of ClCHOO. The destabilization of the *syn*-ClCHOO electronic excited state is apparent in the (unrelaxed) potential energy surfaces along the O–O bond dissociation coordinate shown in Figure 9. The $S_0$ and $S_2$ potentials of both conformers are plotted relative to the ground state minimum (0 eV) of *syn*-ClCHOO. The $S_2$ state of *anti*-ClCHOO has lower energy across the Frank Condon region. The mild $\pi$-electron donation afforded by a chorine substituent extends the conjugation from a 4-electron $\pi$ system to a 6-electron $\pi$ system when compared with $CH_2OO$, thus promoting a bathochromic (longer wavelength, lower energy) shift in electronic absorption. This shift is evident in the experimental spectrum as well as the VEE of *anti*-ClCHOO. The nonbonding effects, which characterize the ground electronic state of *syn*-ClCHOO as both more stable and similar to $CH_2OO$ when compared to *anti*-ClCHOO, stabilize the valence orbitals and destabilize the antibonding orbitals. Consequently, these effects results in a larger $S_2$–$S_0$ energy gap. This is evident in the CASSCF(12/9) energy difference of the $\pi^* — \pi$ (HOMO–LUMO) natural orbitals, where the *syn*-ClCHOO energy gap is 0.5 eV higher than that of *anti*-ClCHOO. The relative destabilization of the excited electronic state of *syn*-ClCHOO causes greater mixing with higher lying electronic states with $\sigma^* \leftarrow$ n character. This is reflected in the CI coefficients in which the *syn*-ClCHOO has an order of magnitude greater electronic character associated with $\sigma^* \leftarrow$ n compared to *anti*-ClCHOO in the $S_2$ state (Table 3). A comprehensive list of electronic configuration contributions is given in Table S4. The greater $\pi^* \leftarrow \pi$ orbital energy gap in *syn*-ClCHOO leads to the relative hypsochromic (shorter wavelength, higher energy) shift observed in electronic absorption.

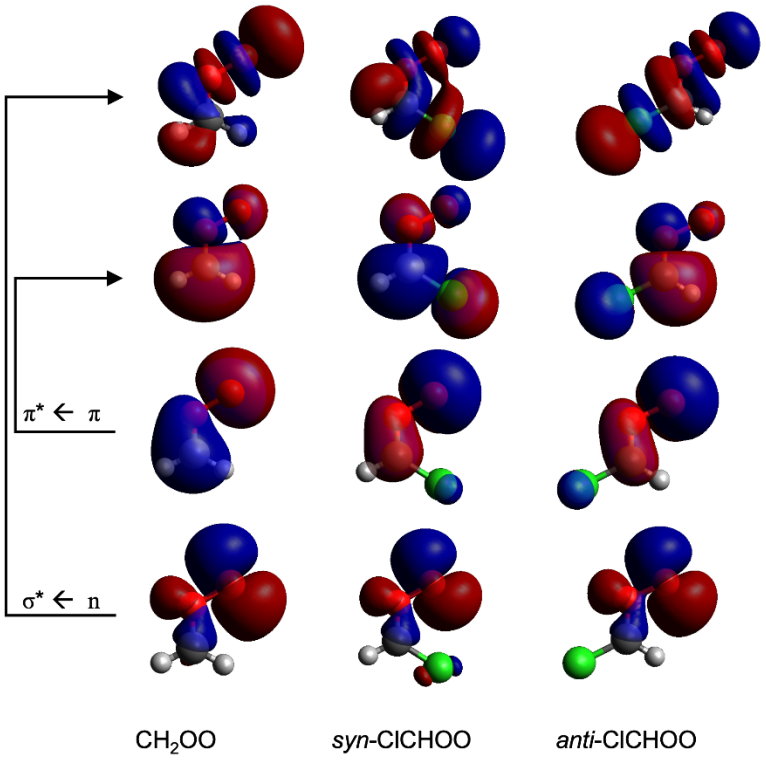


**Figure 8.** Natural molecular orbitals involved in the optically bright transition, which is dominated by the $\pi^* \leftarrow \pi$ transition, for $CH_2OO$ (left), *syn*-ClCHOO (middle), and *anti*-ClCHOO (right).

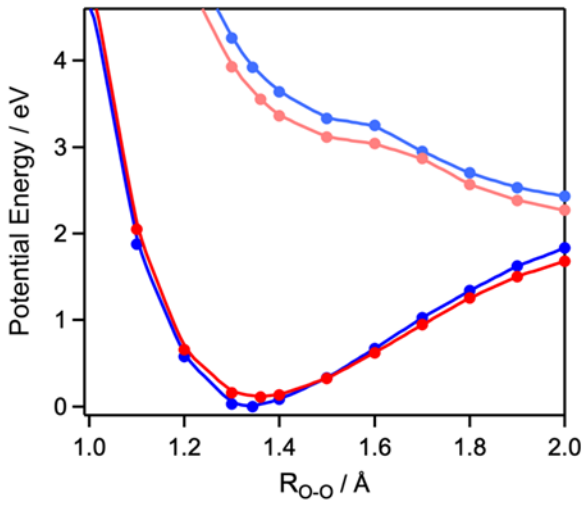


**Figure 9.** Potential energy curves (unrelaxed) computed along the O–O bond dissociation coordinate for the ground and optically bright $S_2$ states for *syn*- (blue) and *anti*-ClCHOO (red).

**Table 3.** Contributions associated with selected excitations based on CASSCF(10/8) and CASSCF(12/9) calculations for $CH_2OO$ and ClCHOO, respectively. CI coefficients are presented as percentage of total electronic character associated with the ground ($S_0$) and optically bright ($S_2$) electronic states.

| Configuration | Ground State | | $\pi^* \leftarrow \pi$ | | $\sigma^* \leftarrow n$ | |
|---|---|---|---|---|---|---|
| Electronic state | $S_0$ | $S_2$ | $S_0$ | $S_2$ | $S_0$ | $S_2$ |
| $CH_2OO$ | 61.9 | 22.5 | 28.9 | 57.8 | 0.17 | 4.3 |
| *syn*-ClCHOO | 63.8 | 20.3 | 25.4 | 56.2 | 0.13 | 2.8 |
| *anti*-ClCHOO | 59.0 | 24.0 | 30.5 | 55.0 | 0.01 | 0.66 |

## Conclusions

The singly chlorinated Criegee intermediate, ClCHOO, has been characterized on the strong $\pi^* \leftarrow \pi$ electronic transition. The electronic spectrum of ClCHOO has been recorded using UV-vis induced depletion of the VUV photoionization signal on the mass channel m/z = 80. The resultant electronic spectrum from 295 to 409 nm is symmetric and broad, and peaks at 350 nm. Multireference calculations yield vertical transition energies and oscillator strengths for transitions to the $S_2$ states for the two conformers of the chlorinated Criegee intermediate, *syn*-ClCHOO and *anti*-ClCHOO, as well as the simplest Criegee intermediate, $CH_2OO$. A nuclear ensemble simulation method along with previous jet-cooled microwave studies are used to assign the spectrum to both the *syn* and *anti* conformers of ClCHOO.[16] Theory predicts similar VEEs for $CH_2OO$ and *syn*-ClCHOO, while the *anti* conformer exhibits a significant (~40 nm) shift to longer wavelengths. The latter is due to extended conjugation afforded by the π donation of the chlorine substituent, resulting in a bathochromic shift. While *syn*-ClCHOO also exhibits extended π conjugation associated with the optically bright electronic state, a larger HOMO–LUMO energy gap and considerable $\sigma^*$ and n electronic character will hypsochromically shift the $S_2 \leftarrow S_0$ transition. High-level ground state calculations also predict a significant difference in the

relative stability of conformers, and NBO analysis shows that hyperconjugative-like interactions play a role in the energetic stability of ClCHOO and $CH_2OO$.

Supporting Information includes description of synthetic method, active spaces used in multireference calculations, additional multireference calculations, and optimized geometry of relevant species.

Acknowledgements
Research in the Lester group was supported by the National Science Foundation under grant CHE-2301298. This work used the Advanced Cyberinfrastructure Coordination Ecosystem: Service & Support (ACCESS) program, which is supported by National Science Foundation grants #2138259, #2138286, #2138307, #2137603, and #2138296, through the allocation TG-CHE190088. M.C.K. is grateful to the NSF (CHE-2400215) for financial support of this research. Partial instrumentation support (NMR spectrometer) was provided by NSF CHE-1827457 and the Vagelos Institute for Energy Science and Technology. T.N.V.K. is grateful to the NSF (CHE-2003422) for funding. The authors thank Craig Murray (University of California, Irvine) for sharing the transient absorption data of ClCHOO from Reference 20.

References


1. Beames, J. M.; Liu, F.; Lu, L.; Lester, M. I. Ultraviolet Spectrum and Photochemistry of the Simplest Criegee Intermediate $CH_2OO$. *J. Am. Chem. Soc.* **2012**, *134*, 20045-20048.
2. Barber, V. P.; Pandit, S.; Green, A. M.; Trongsiriwat, N.; Wash, P. J.; Klippenstein, S. J.; Lester, M. I. Four-Carbon Criegee Intermediate from Isoprene Ozonolysis: Methyl Vinyl Ketone Oxide Synthesis, Infrared Spectrum, and OH Production. *J. Am. Chem. Soc.* **2018**, *140*, 10866-10880.
3. Vansco, M. F.; Marchetti, B.; Trongsiriwat, N.; Bhagde, T.; Wang, G. H.; Walsh, P. J.; Klippenstein, S. J.; Lester, M. I. Synthesis, Electronic Spectroscopy, and Photochemistry of Methacrolein Oxide: A Four-Carbon Unsaturated Criegee Intermediate from Isoprene Ozonolysis. *J. Am. Chem. Soc.* **2019**, *141*, 15058-15069.
4. Arneth, A.; Monson, R. K.; Schurgers, G.; Niinemets, Ü.; Palmer, P. I. Why are estimates of global terrestrial isoprene emissions so similar (and why is this not so for monoterpenes)? *Atmos. Chem. Phys.* **2008**, *8*, 4605-4620.
5. Beames, J. M.; Liu, F.; Lu, L.; Lester, M. I. UV spectroscopic characterization of an alkyl substituted Criegee intermediate $CH_3CHOO$. *J. Chem. Phys.* **2013**, *138*, 244307.
6. Liu, F.; Beames, J. M.; Green, A. M.; Lester, M. I. UV Spectroscopic Characterization of Dimethyl- and Ethyl-Substituted Carbonyl Oxides. *J. Phys. Chem. A.* **2014**, *118*, 2298-2306.
7. Watson, N. A. I.; Beames, J. M. Bimolecular sinks of Criegee intermediates derived from hydrofluoroolefins - a computational analysis. *Environ. Sci. Atmos.* **2023**, *3*, 1460–1484.
8. Caravan, R. L.; Vansco, M. F.; Lester, M. I. Open questions on the reactivity of Criegee intermediates. *Commun. Chem.* **2021**, *4*, 44.
9. Vansco, M. F.; Zou, M. J.; Antonov, I. O.; Ramasesha, K.; Rotavera, B.; Osborn, D. L.; Georgievskii, Y.; Percival, C. J.; Klippenstein, S. J.; Taatjes, C. A. et al. Dramatic Conformer-Dependent Reactivity of the Acetaldehyde Oxide Criegee Intermediate with Dimethylamine *Via* a 1,2-Insertion Mechanism. *J. Phys. Chem. A.* **2022**, *126*, 710-719.
10. Cox, R. A.; Ammann, M.; Crowley, J. N.; Herrmann, H.; Jenkin, M. E.; McNeill, V. F.; Mellouki, A.; Troe, J.; Wallington, T. J. Evaluated kinetic and photochemical data for atmospheric chemistry: Volume VII - Criegee intermediates. *Atmos. Chem. Phys.* **2020**, *20*, 13497-13519.
11. David, L. M.; Barth, M.; Höglund-Isaksson, L.; Purohit, P.; Velders, G. J. M.; Glaser, S.; Ravishankara, A. R. Trifluoroacetic acid deposition from emissions of HFO-1234yf in India, China, and the Middle East. *Atmos. Chem. Phys.* **2021**, *21*, 14833-14849.
12. Salierno, G. On the Chemical Pathways Influencing the Effective Global Warming Potential of Commercial Hydrofluoroolefin Gases. *ChemSusChem.* **2024**, e202400280.
13. Mcgillen, M. R.; Fried, Z. T. P.; Khan, M. A. H.; Kuwata, K. T.; Martin, C. M.; O'Doherty, S.; Pecere, F.; Shallcross, D. E.; Stanley, K. M.; Zhang, K. X. Ozonolysis can produce long-lived greenhouse gases from commercial refrigerants. *P. Natl. Acad. Sci. U.S.A.* **2023**, *120*.
14. Kumar, M.; Francisco, J. S. Reactions of Criegee Intermediates with Non-Water Greenhouse Gases: Implications for Metal Free Chemical Fixation of Carbon Dioxide. *J. Phys. Chem. Lett.* **2017**, *8*, 4206-4213.
15. Kumar, M.; Francisco, J. S. H-X (X = H, $CH_3$, $CH_2F$, $CHF_3$, and $SiH_3$) Bond Activation by Criegee Intermediates: A Theoretical Perspective. *J. Phys. Chem. A.* **2017**, *121*, 9421-9428.
16. Cabezas, C.; Guillemin, J. C.; Endo, Y. Fourier-transform microwave spectroscopy of a halogen substituted Criegee intermediate ClCHOO. *J. Chem. Phys.* **2016**, *145*, 184304.
17. Karsili, T. N. V.; Marchetti, B.; Lester, M. I.; Ashfold, M. N. R. Electronic Absorption Spectroscopy and Photochemistry of Criegee Intermediates. *Photochem. Photobiol.* **2023**, *99*, 4-18.
18. Kuwata, K. T. Computational Modeling of the Conformation-Dependent Atmospheric Reactivity of Criegee Intermediates. *J. Phys. Chem. A.* **2024**, *128*, 7331-7345.
19. Chhantyal-Pun, R.; Khan, M. A. H.; Taatjes, C. A.; Percival, C. J.; Orr-Ewing, A. J.; Shallcross, D. E. Criegee intermediates: production, detection and reactivity. *Int. Rev. Phys. Chem.* **2020**, *39*, 383-422.

20. Kapnas, K. M.; Toulson, B. W.; Foreman, E. S.; Block, S. A.; Hill, J. G.; Murray, C. UV photodissociation dynamics of $CHI_2Cl$ and its role as a photolytic precursor for a chlorinated Criegee intermediate. *Phys. Chem. Chem. Phys.* **2017**, *19*, 31039-31053.
21. Li, D. B.; Ng, S. C.; Novak, I. Novel synthetic approaches to CHBrFI, CHClFI and CHBrClI. *Tetrahedron.* **2002**, *58*, 5923-5926.
22. Vansco, M. F.; Marchetti, B.; Lester, M. I. Electronic spectroscopy of methyl vinyl ketone oxide: A four-carbon unsaturated Criegee intermediate from isoprene ozonolysis. *J. Chem. Phys.* **2018**, *149*, 244309.
23. Liu, F.; Beames, J. M.; Petit, A. S.; McCoy, A. B.; Lester, M. I. Infrared-driven unimolecular reaction of $CH_3CHOO$ Criegee intermediates to OH radical products. *Science.* **2014**, *345*, 1596-1598.
24. Liu, F.; Beames, J. M.; Lester, M. I. Direct production of OH radicals upon CH overtone activation of $(CH_3)_2COO$ Criegee intermediates. *J. Chem. Phys.* **2014**, *141*, 234312.
25. *Gaussian 16 Rev. C.01*; Frisch, M. J.; Trucks, G. W.; Schlegel, H. B.; Scuseria, G. E.; Robb, M. A.; Cheeseman, J. R.; Scalmani, G.; Barone, V.; Petersson, G. A.; Nakatsuji, H. et al.; Wallingford, CT, 2016.
26. *NBO Version 3.1*; E. D. Glendening, A. E. R., J. E. Carpenter, F. Weinhold.
27. Werner, H.-J.; Knowles, P. J.; Knizia, G.; Manby, F. R.; Schütz, M.; Celani, P.; Györffy, W.; Kats, D.; Korona, T.; Lindh, R. et al. *MOLPRO, a Package of ab initio Programs*. 2022. https://www.molpro.net (accessed 14 October 2024).
28. Werner, H. J.; Knowles, P. J.; Knizia, G.; Manby, F. R.; Schütz, M. Molpro: a general-purpose quantum chemistry program package. *Wires. Comput. Mol. Sci.* **2012**, *2*, 242-253.
29. Werner, H. J.; Knowles, P. J.; Manby, F. R.; Black, J. A.; Doll, K.; Hesselmann, A.; Kats, D.; Köhn, A.; Korona, T.; Kreplin, D. A. et al. The Molpro quantum chemistry package. *J. Chem. Phys.* **2020**, *152*, 144107.
30. Adler, T. B.; Knizia, G.; Werner, H. J. A simple and efficient CCSD(T)-F12 approximation. *J. Chem. Phys.* **2007**, *127*, 221106.
31. Gyorffy, W.; Shiozaki, T.; Knizia, G.; Werner, H. J. Analytical energy gradients for second-order multireference perturbation theory using density fitting. *J. Chem. Phys.* **2013**, *138*, 104104.
32. Kreplin, D. A.; Knowles, P. J.; Werner, H. J. Second-order MCSCF optimization revisited. I. Improved algorithms for fast and robust second-order CASSCF convergence. *J. Chem. Phys.* **2019**, *150*, 194106.
33. McCoy, J. C.; Marchetti, B.; Thodika, M.; Karsili, T. N. V. A Simple and Efficient Method for Simulating the Electronic Absorption Spectra of Criegee Intermediates: Benchmarking on $CH_2OO$ and $CH_3CHOO$. *J. Phys. Chem. A.* **2021**, *125*, 4089-4097.
34. Barbatti, M.; Ruckenbauer, M.; Plasser, F.; Pittner, J.; Granucci, G.; Persico, M.; Lischka, H. Newton-X: a surface-hopping program for nonadiabatic molecular dynamics. *Wires. Comput. Mol. Sci.* **2014**, *4*, 26-33.
35. Barbatti, M.; Granucci, G.; Persico, M.; Ruckenbauer, M.; Vazdar, M.; Eckert-Maksic, M.; Lischka, H. The on-the-fly surface-hopping program system NEWTON-X: Application to ab initio simulation of the nonadiabatic photodynamics of benchmark systems. *J. Photoch. Photobio. A.* **2007**, *190*, 228-240.
36. Esposito, V. J.; Werba, O.; Bush, S. A.; Marchetti, B.; Karsili, T. N. V. Insights into the Ultrafast Dynamics of $CH_2OO$ and $CH_3CHOO$ Following Excitation to the Bright $^1\pi\pi^*$ State: The Role of Singlet and Triplet States. *Photochem. Photobiol.* **2022**, *98*, 763-772.
37. Wang, G. H.; Liu, T. L.; Zou, M. J.; Karsili, T. N. V.; Lester, M. I. UV photodissociation dynamics of the acetone oxide Criegee intermediate: experiment and theory. *Phys. Chem. Chem. Phys.* **2023**, *25*, 7453-7465.
38. Lehman, J. H.; Li, H. W.; Beames, J. M.; Lester, M. I. Communication: Ultraviolet photodissociation dynamics of the simplest Criegee intermediate $CH_2OO$. *J. Chem. Phys.* **2013**, *139*, 141103.
39. Li, H. W.; Fang, Y.; Kidwell, N. M.; Beames, J. M.; Lester, M. I. UV Photodissociation Dynamics of the $CH_3CHOO$ Criegee Intermediate: Action Spectroscopy and Velocity Map Imaging of O-Atom Products. *J. Phys. Chem. A.* **2015**, *119*, 8328-8337.

40. Liu, T. L.; Zou, M. J.; Caracciolo, A.; Sojdak, C. A.; Lester, M. I. Substituent Effects on the Electronic Spectroscopy of Four-Carbon Criegee Intermediates. *J. Phys. Chem. A.* **2022**, *126*, 6734–6741.
41. Li, H. W.; Fang, Y.; Beames, J. M.; Lester, M. I. Velocity map imaging of O-atom products from UV photodissociation of the $CH_2OO$ Criegee intermediate. *J. Chem. Phys.* **2015**, *142*.
42. Antwi, E.; Bush, R. E.; Marchetti, B.; Karsili, T. N. V. A direct dynamics study of the exotic photochemistry of the simplest Criegee intermediate, $CH_2OO$. *Phys. Chem. Chem. Phys.* **2022**, *24*, 16724-16731.
43. Poirier, C. A.; Guidry, L. M.; Ratliff, J. M.; Esposito, V. J.; Marchetti, B.; Karsili, T. N. V. Modeling the Ground- and Excited-State Unimolecular Decay of the Simplest Fluorinated Criegee Intermediate, HFCOO, Formed from the Ozonolysis of Hydrofluoroolefin Refrigerants. *J. Phys. Chem. A.* **2023**, *127*, 6377-6384.
44. Ting, W. L.; Chen, Y. H.; Chao, W.; Smith, M. C.; Lin, J. J. M. The UV absorption spectrum of the simplest Criegee intermediate $CH_2OO$. *Phys. Chem. Chem. Phys.* **2014**, *16*, 10438-10443.
45. Anglada, J. M.; González, J.; Torrent-Sucarrat, M. Effects of the substituents on the reactivity of carbonyl oxides. A theoretical study on the reaction of substituted carbonyl oxides with water. *Phys. Chem. Chem. Phys.* **2011**, *13*, 13034-13045.
46. Gutbrod, R.; Kraka, E.; Schindler, R. N.; Cremer, D. Kinetic and theoretical investigation of the gas-phase ozonolysis of isoprene: Carbonyl oxides as an important source for OH radicals in the atmosphere. *J. Am. Chem. Soc.* **1997**, *119*, 7330-7342.
47. Bunnelle, W. H. Preparation, Properties, and Reactions of Carbonyl Oxides. *Chem. Rev.* **1991**, *91*, 335-362.
48. Nakajima, M.; Endo, Y. Communication: Determination of the molecular structure of the simplest Criegee intermediate $CH_2OO$. *J. Chem. Phys.* **2013**, *139*, 101103.
49. Sheps, L.; Scully, A. M.; Au, K. UV absorption probing of the conformer-dependent reactivity of a Criegee intermediate $CH_3CHOO$. *Phys. Chem. Chem. Phys.* **2014**, *16*, 26701-26706.

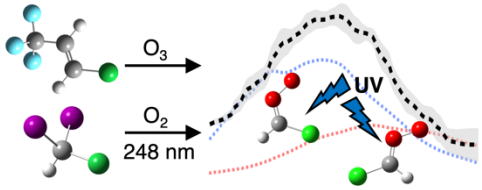


TOC Graphic